

Jahn-Teller driven quadrupolar ordering and spin-orbital dimer formation in GaNb_4Se_8

Tsung-Han Yang,^{1,*} Tieyan Chang,² Yu-Sheng Chen,² and K. W. Plumb^{1,†}

¹*Department of Physics, Brown University, Providence, RI 02912, USA*

²*NSF's ChemMatCARS Beamline, The University of Chicago, Advanced Photon Source, Argonne, Illinois 60439, United States*

(Dated: January 10, 2024)

The lacunar spinel GaNb_4Se_8 is a tetrahedral cluster Mott insulator where spin-orbit coupling on molecular orbitals and Jahn-Teller energy scales are competitive. GaNb_4Se_8 undergoes a structural and anti-polar ordering transition at $T_Q = 50$ K that corresponds to a quadrupolar ordering of molecular orbitals on Nb_4 clusters. A second transition occurs at $T_M = 29$ K, where local distortions on the Nb_4 clusters rearrange. We present a single crystal x-ray diffraction investigation of these phase transitions and solve the crystal structure in the intermediate $T_M < T < T_Q$ and low $T < T_M$ temperature phases. The intermediate phase is a primitive cubic $P2_13$ structure with a staggered arrangement of Nb_4 cluster distortions. A symmetry mode analysis reveals that the transition at T_Q is continuous and described by a single Jahn-Teller active amplitude mode. In the low temperature phase, the symmetry of Nb_4 clusters is further reduced and the unit cell doubles into an orthorhombic $P2_12_12_1$ space group. Nb_4 clusters rearrange through this transition to form a staggered arrangement of intercluster dimers, suggesting a valence bond solid magnetic state.

INTRODUCTION

The many interesting properties of strongly correlated magnetic materials arise from an interplay of charge, spin, orbital, and lattice degrees of freedom. In transition metal materials, it is often the case that spin and orbital effects appear in a hierarchy of well separated energy scales and can be considered to act independently of each other. For example, in transition metal materials that have an orbital degeneracy, the orbital degrees of freedom are typically quenched out via a Jahn-Teller mechanism at a high temperature relative to the magnetic ordering temperatures, rendering a spin only magnetic model. However, for 4d or 5d transition metal materials, relativistic spin-orbit coupling can significantly alter this energy hierarchy, giving rise to magnetic phases with spin-orbital entangled degrees of freedom. The presence of such spin-orbital degrees of freedom dramatically influences magnetic ground states and are the essential microscopic ingredient to stabilize, for example, Kitaev spin liquids, topological superconductors, or spin-orbital liquid phases depending on the particular electron filling [1–5]. In particular, 4d¹ or 5d¹ Mott insulators, with a single electron occupying the $j = 3/2$ spin-orbital state have attracted significant attention [3, 6–9] as materials where multipolar orders or spin-orbital liquids may be realized.

Lacunar spinels with the chemical formula GaM_4X_8 ($M = \text{V}, \text{Nb}, \text{Ta}$; $X = \text{S}, \text{Se}$) are a family of cluster Mott insulators that contain a single unpaired electron occupying molecular t_2 orbitals on each M_4 cluster site [Fig. 1 (a)] [10, 11]. The isostructural members of this family that contain 3d, 4d, and 5d transition metals respectively provide an ideal opportunity to investigate the interplay of spin, orbit, and lattice degrees of freedom as atomic spin-

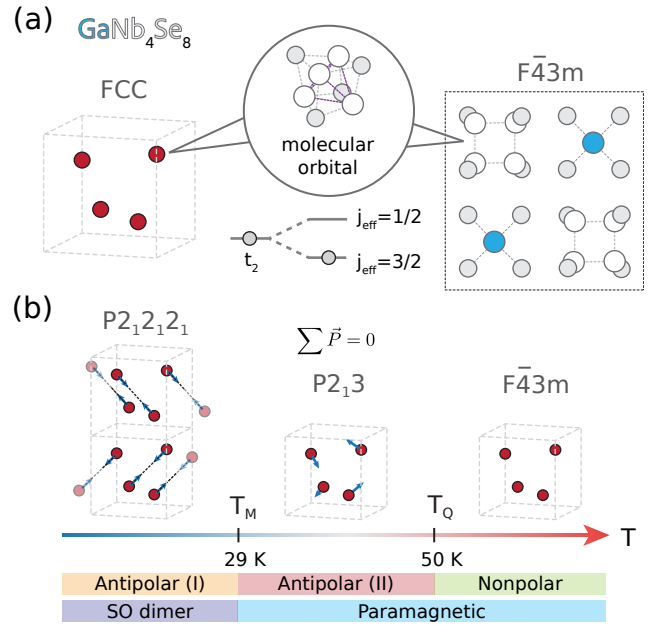


FIG. 1. (a) Crystal structure and molecular orbital level scheme GaNb_4Se_8 . The correlated units are molecular $j_{\text{eff}} = 3/2$ orbitals on Nb_4Se_4 cubane units. Each Nb_4 cluster occupies an FCC lattice site. (b) Structural, magnetic, and polar phases transitions in GaNb_4Se_8 at different temperatures. The total polarization for two antipolar phases are zero while the internal arrangements differ.

orbit coupling and correlations are systematically varied. Indeed, clear trends in the relative separation of spin and orbital energy scales are observed across the series. In GaV_4S_8 and GaV_4Se_8 the orbital degrees of freedom are quenched through a high temperature Jahn-Teller (JT) distortion that is preceded by spin ordering at lower temperatures [12, 13]. The JT distortion generated an elec-

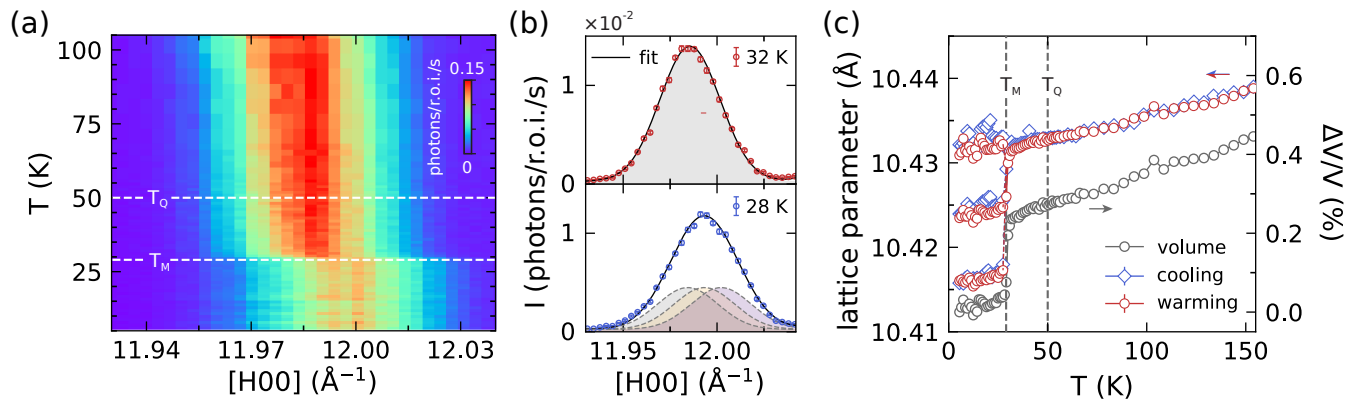


FIG. 2. (a) Temperature-dependent single crystal x-ray diffraction of the cubic $[12, 0, 0]$ Bragg reflection in GaNb_4Se_8 . The $[12, 0, 0]$ reflection is not sensitive to the transition at T_Q but displays a clear shift and broadening below T_M in the orthorhombic cell phase. (b) Gaussian fits of the $[12, 0, 0]$ reflection above and below T_M . The peak width is fixed to instrumental resolution for the fit below T_M . (c) Temperature dependent lattice parameter(s) and the cell volume extracted from $[12, 0, 0]$ reflection.

tric dipole moment on each V_4 cluster that is oriented uniformly along the same direction for each cluster resulting in a ferro-polar ordering [14–18]. On the other hand, in those compounds where spin-orbit coupling is the strongest, GaNb_4S_8 and GaTa_4Se_8 , there is only a single magneto-structural transition leading to a dimerized, valence bond solid, ground state [19, 20]. The single transition, simultaneously involving spin and orbital degrees of freedom implies a vanishing separation between spin and orbital energy scales. Indeed, in GaTa_4Se_8 , the correlated units are molecular spin-orbit entangled $j_{\text{eff}} = 3/2$ [10, 21–23] degrees of freedom. In such a spin-orbital state, JT effects are suppressed, but substantial spin-orbital dynamics are reflected in the disorder-order nature of the spin-orbital transition and corresponding phonon anomaly above the transition [22]. The structural distortions in GaNb_4S_8 and GaTa_4Se_8 also generate electric dipoles on the transition metal clusters, but in these materials the distortions arrange in a staggered or anti-ferro polar ordering [17, 22, 24, 25].

GaNb_4Se_8 presents an interesting intermediate regime where spin-orbit coupling and JT energy scales are on more equal footing. In this material, there is a cubic-to-cubic structural phase transition at $T_Q = 50$ K preceding a magneto structural distortion [20, 25, 26] and the formation of structural dimers at $T_M = 29$ K, illustrated in Fig. 1. The cubic-to-cubic structural distortion is associated with an anomaly in the temperature dependent dielectric constant [25] and the intermediate state suggests the possibility for anti-ferro electric quadrupolar ordering of $j = 3/2$ spin-orbital degrees of freedom [20]. An additional anomaly of the dielectric constant at T_M suggests a second rearrangement of electric quadrupoles at this temperature [25]. However, the precise form of quadrupolar ordering and underlying mechanism in GaNb_4Se_8 have not been resolved because the crystal structures and atomic positions associated

with the phases for $T_M < T < T_Q$ and $T < T_M$ are not known. This difficulty arises because of weak diffraction intensities from low temperature superlattice structural peaks, hindering the refinement of powder diffraction measurements, and from complications from domains in the low temperature orthorhombic unit cell. Detailed knowledge of the crystal structure, and especially the transition metal atomic positions, is essential to resolve the nature of quadrupolar or orbital ordering in this material and elucidate the microscopic mechanism driving this phenomena.

In this work, we investigate the temperature-dependent crystal structure of GaNb_4Se_8 using synchrotron single crystal x-ray diffraction. We determine the intermediate $T_M < T < T_Q$ and low temperature $T < T_M$ crystal structures of GaNb_4Se_8 and find that the intermediate cubic structure is consistent with previous reports [20]. However, a full refinement of the structure enables a symmetry analysis of the structural transition at T_Q . This analysis reveals it to be continuous (second order) transition described by a single JT active distortion of Nb_4 clusters. At $T_M = 29$ K, GaNb_4Se_8 further undergoes a first order cubic to orthorhombic transition. The unit cell doubles through this transition as Nb_4 clusters rearrange to form structural dimers along cubic (011) directions, consistent with the development of a correlated singlet, or valence bond solid state, that is similar to GaTa_4Se_8 [22]. Our work sheds light on the complex interplay between spin-orbit coupling, lattice distortions, and intercluster interactions to effect electric quadrupolar orderings in Lacunar spinels and provides essential crystal structure information to support further investigation of spin-orbital physics in molecular Mott insulators.

METHODS

Sample Synthesis

Polycrystalline samples of GaNb_4Se_8 were synthesized by solid-state reaction. About 1.5 g of stoichiometric quantities of high-purity raw materials (Gallium: Alfa Aesar, 99.999%; Niobium: Alfa Aesar, 99.99%; Selenium: Alfa Aesar, 99.999%) were loaded into I.D. = 10 mm, 100 mm long quartz ampules under an argon glovebox. The ampules were evacuated, and sealed before heating to 1050 °C with 80 °C/hour ramping rate, held for 24 hours and then air-quenched to room temperature. The resulting powder was reground in an argon glovebox, resealed under vacuum, and heated following the same procedure. Three heating and regrinding repetitions were required to obtain single-phase polycrystalline samples. The composition was confirmed by powder x-ray diffraction (Bruker $\text{Cu K}\alpha$ radiation). Micron scale single crystals of GaNb_4Se_8 were prepared by chemical vapor transport from the phase pure powders. About 1.5 g of single-phase GaNb_4Se_8 powder and 75 mg iodine were sealed in I.D. = 10 mm, 210 mm long quartz ampules. The ampule was placed in a two-zone furnace with 950 °C and 1000 °C zone temperatures for 20 days.

X-ray crystallography

Temperature dependent x-ray diffraction was carried out using a four-circle x-ray diffractometer, Ag $\text{K}\alpha$ radiation, with an XSPeX Lambda 60 K GaAs photon counting detector positioned 78 cm from the sample. The single crystal sample was mounted in reflection geometry on a Cu post on the coldfinger of a closed cycle cryostat for measurements between 3 and 300 K.

Synchrotron crystallography measurements were performed on the 15 ID-D beamline at Advanced Photon Source at Argonne National Laboratory. The sample was mounted on a quartz fiber with epoxy adhesive. We used a 30 keV x-ray beam and Dectris Pilatus3X 1M CdTe area detector with a sample to detector distance of 130 mm for 100 K and 120 mm for 40 K and 20 K measurements. Nitrogen and helium cryo-streams were used to control the sample temperature. For each temperature, diffraction images were collected by rotating the sample through 360 degrees with 0.3 degrees/step for 100 K measurements and 0.1 degrees/step for 40 K and 20 K measurements. The images were integrated into reciprocal space and indexed using Bruker APEX4 software. Absorption corrections were applied using SADABS and TWINABS packages and the space group was checked using the XPREP package. Final crystal structure solution and refinements were performed on Shelx with Olex2 user interface [27, 28].

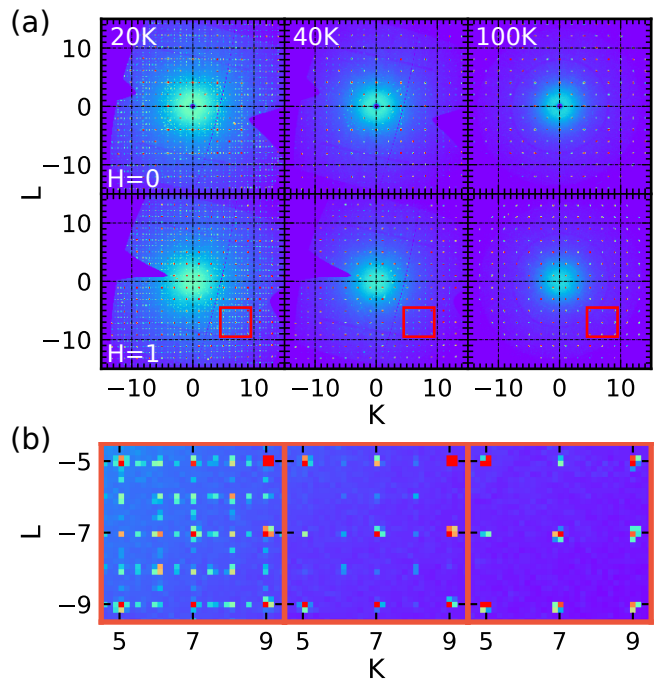


FIG. 3. (a) Reconstruction of (0KL) and (1KL) planes in reciprocal space from x-ray crystallography at 20, 40, and 100 K. (b) Zoomed areas in (1KL) plane, indicated by red boxes in (a), demonstrating the appearance of superlattice reflections.

RESULTS

Jahn-Teller driven antiferro quadrupolar order

We first investigate the structural phase transition at $T_Q = 50$ K. Temperature-dependent diffraction measurements of a cubic $[12, 0, 0]$ Bragg peak are shown in Fig. 2. The cubic peak exhibits noticeable broadening at $T_M = 29$ K, but no detectable change across T_Q [Fig. 2 (a)], consistent with a cubic-cubic phase transition. The temperature dependent lattice parameters and cell volume extracted from Gaussian fits of a longitudinal cut through the $[12, 0, 0]$ peak are shown in Fig. 2 (c), demonstrating a continuous variation across T_Q , consistent with the second order nature of this transition.

Synchrotron x-ray crystallography at 40 K reveals a primitive cubic unit cell and space group $P2_13$. Fig. 3 shows the appearance of reflections for $h+k=2n$; $h+l=2n$; $k+l=2n$ that violate reflection condition for a face-center-cubic (FCC) cell and indicate a primitive cubic unit cell at 40 K. Our refinement gives the best fit to the $P2_13$ space group with $R_1 = 0.0442$ ($I \geq 2\sigma$). Nb atoms sit on 16e Wyckoff positions (WP) in the high temperature cubic phase that split into 4a and 12b WPs in the $P2_13$ structure resulting in an elongation of Nb_4 tetrahedra along the cubic $\langle 111 \rangle$ directions as shown in Fig. 5 (a) and (b). Parameters of the refinement are

listed in Table III and the refined atomic positions are listed in the supplementary materials [29]. The space group and refined structure exhibiting a staggered arrangement of Nb₄ cluster distortions are consistent with anti-ferro quadrupolar ordering previously proposed in this regime [20, 25].

We find that the transition at T_Q is second order, consistent with the absence of any detectable volume change or hysteresis through the transition [Fig. 2 (c)], and a single irreducible representation order parameter for the distortion. The second order nature is apparent in Fig. 4, that shows the continuous onset of the [8, 0, 1] reflection intensity at T_Q. This Bragg reflection is directly related to a single amplitude mode order parameter [Fig. 5 (b)] identified for this structural transition.

A symmetry mode analysis through the cubic-cubic F43m→P2₁3 distortion was carried out using the Bilbao crystallographic server [30–32] to yield the primary mode amplitudes and isotropy space groups listed in Table I. Corresponding atomic distortions for each symmetry mode are listed in supplementary materials [29]. The structural transition at T_Q is described by two primary distortions: Γ₁, that belongs to the F43m, and a dominant JT active X₅ mode, that belongs to P2₁3 and acts to distort Nb₄ clusters along $\langle\bar{1}11\rangle$ directions as shown in Fig. 5 (a) and (b). This second-order transition at T_Q can be naturally described as a continuous increase of the X₅ mode amplitude order parameter [Fig. 5 (b)] that leads to the development of quadrupolar moments on Nb₄ clusters. Thus, a JT distortion of Nb₄ clusters underlies staggered quadrupolar ordering at T_Q in GaNb₄Se₈, similar to the proposed JT mechanism driving antipolar order in GaNb₄S₈ [17]. However, it is interesting that in GaNb₄Se₈ the transition at T_Q solely involves the ordering of structural (orbital) degrees-of-freedom, while magnetic and structural degrees of freedom undergo a second simultaneous transition at lower temperatures T_M < T_Q. This separation of energy scales is distinct from GaNb₄S₈ and GaTa₄Se₈ where there is only one and single transition involving the structural and magnetic degrees of freedom.

TABLE I. Irreducible representation of distortion modes for F43m to P2₁3 transition, amplitudes are normalized to the primitive unit cell of the high-symmetry F43m structure.

\vec{K}	Irrep	Direction	Isotropy SG	Amp. (Å)
(0,0,0)	Γ ₁	(a)	F43m	0.0037
(0,1,0)	X ₅	(a,a,a,a,a)	P2 ₁ 3	0.0826

Structural dimers in the antipolar II ordered phase

We now examine the evolution of the crystal structure through the first-order phase transition at T_M = 29 K,

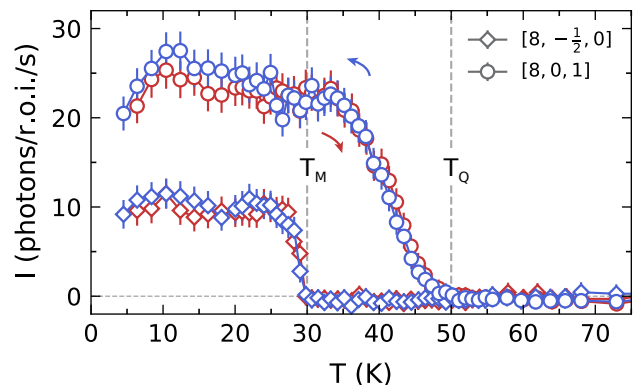


FIG. 4. Temperature-dependent peak intensities of and [8, 0, 1] Bragg peak that represents the order parameter for the F43m to P2₁3 structural transition at T_Q=50 K, and [8, - $\frac{1}{2}$, 0] reflection that shows a unit cell doubling through the first order transition at T_M=29 K.

where a simultaneous structural transition and reduction in the temperature dependent magnetization occur. As shown in Fig. 3 and Fig. 4, superlattice Bragg reflections, at $[\frac{1}{2}, 0, 0]$ positions of the cubic cell, appear upon cooling below T_M. These indicate a unit cell doubling along one axis through a cubic to orthorhombic structural transition, similar to what has been observed in GaNb₄S₈ [17] and GaTa₄Se₈ [22]. The first order nature of this transition is identified through a discontinuous change in lattice parameters and cell volume [Fig. 2 (c)], a discontinuous onset of superlattice reflection intensity [Fig. 4], and sharp, divergent, heat capacity [25].

In order to account for the formation of structural domains through this transition, we define four twinned cells for each doubled axis along the crystallographic **a**, **b**, or **c** axis by rotating against the doubled axis through 0, 90, 180, and 270 degrees; giving 12 domains in total. Integrated intensities of Bragg reflections were corrected based on symmetry operations using TWINABS for these 12 domains. After accounting for the domain structure, our crystallographic refinement gives the best agreement with a unit cell doubled orthorhombic P2₁2₁2₁ space group with R₁ = 0.0855 (I ≥ 2σ). Refinement parameters are listed in Table III, and the refined structure is shown in Fig. 5 (c) and (d).

Fig. 5 (c) and (d) show the refined crystal structure and refined atomic positions are listed in the supplementary materials [29]. At T_M, Nb₄ clusters distort so that each tetrahedron elongate along cubic $\langle 011 \rangle$ or equivalent directions [Fig. 5 (c)] and has three inequivalent bond lengths as illustrated in Fig. 5 (d). Distorted Nb₄ tetrahedra rearrange so that each points towards a single neighboring cluster, forming structural dimers along $\langle 011 \rangle$ or $\langle 0\bar{1}1 \rangle$ directions as indicated in Fig. 5 (c). The symmetry reduction on Nb₄ tetrahedra must have an associated reorientation of the polar axis, and their stag-

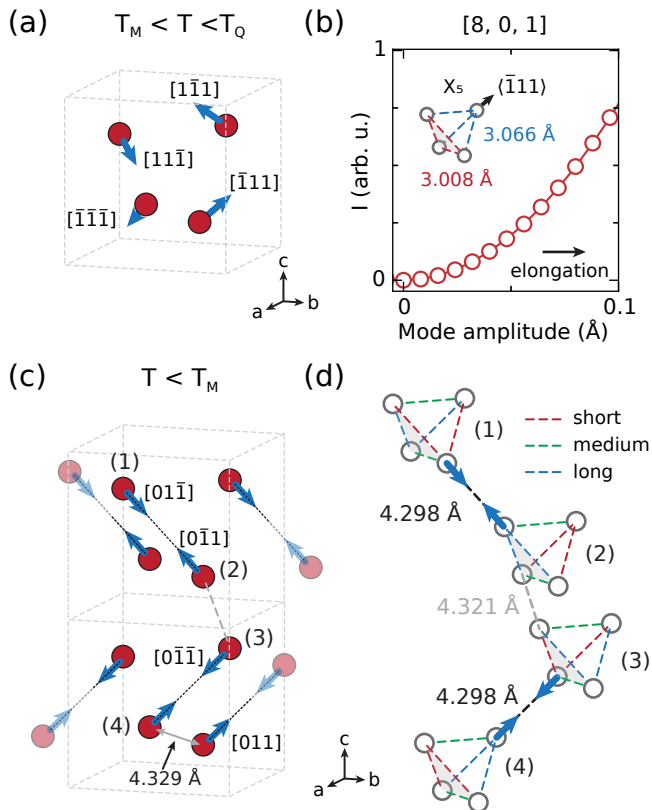


FIG. 5. (a) Schematic representation of Nb₄ tetrahedron distortions in the T=40 K refined crystal structure. Red circles represent Nb₄ clusters, and blue arrows indicate the direction of overall distortion on each cluster in the cubic cell. (b) Simulated [8,0,1] peak intensity (using Dans Diffraction package [33]) and distortion on each Nb₄ cluster. The intensity of a [8,0,1] structural Bragg peak continuously increases with the X₅ distortion, as Nb₄ clusters elongate along $\langle 111 \rangle$ directions of the cubic P₂₁3 cell. (c) Schematic of Nb₄ cluster distortions in the orthorhombic P₂₁2₁2₁ cell at 20 K. Black dashed lines indicate the closest distance between neighboring clusters, showing a dimerized structure. (d) Schematic of the distortion of Nb₄ clusters. The location of each cluster within the orthorhombic cell are labeled with corresponding numbers in (c). Each cluster has two long bonds (blue), two short bonds (red) and two intermediate bonds (green).

gered arrangement indicates an antipolar ordering. Thus, the crystal structures reported here are consistent with the two successive antipolar orderings found at T_Q and T_M in GaNb₄Se₈ [25], and reveal the nature of those orderings. The structural dimer motif and vanishing magnetization at T_M [20, 25] also suggest magnetic singlets form across intercluster dimers as GaNb₄Se₈ enters a valence bond crystal like state below T_M, similar to what has been observed in GaTa₄Se₈ [22].

The unit cell doubled P₂₁2₁2₁ structure is not a subgroup of the intermediate P₂₁3 structure and the transition at T_M cannot be described in terms of a JT active mode as for that at T_Q. The 1×1×1 orthorhom-

bic P₂₁2₁2₁ is the exclusive sub group of the intermediate P₂₁3 structure, while the superlattice reflections indicate the structure is a 1×1×2 cell [Fig. 3]. Therefore, in order to better interrogate the mechanisms that underlie this transition, we compute structure relations against the high temperature F43m structure to obtain irreducible representations and distortion mode amplitudes listed in Table II. The distortion again involves a JT active X₅ mode, but in this case there are other unit cell doubling distortions of comparable magnitude that modulate intercluster bonds and mix with the JT active modes. The necessity of multiple distortion modes to describe the transition at T_M is consistent with the involvement of more than one order parameter including at least structural and magnetic degrees of freedom, and indicates that a JT mechanism is not the origin of the transition at T_M. An involvement of distortions that modulate intercluster bonds, and the formation of magnetic singlets indicates that the transition at T_M may instead be driven by intercluster interactions, similar to GaTa₄Se₈ [22].

TABLE II. Irreducible representation of distortion modes for F43m to P₂₁2₁2₁ transition, amplitudes are normalized to the primitive unit cell of the high-symmetry F43m structure.

\vec{K}	Irrep	Direction	Isotropy SG	Amp. (Å)
(0,0,0)	Γ_1	(a)	F43m	0.0045
(0,0,0)	Γ_3	(a,b)	F222	0.0035
$(0, \frac{1}{2}, 0)$	$\Delta_3\Delta_4$	(0,0,0,a,b,0,0,0,-b,a)	C222 ₁	0.0697
(0,1,0)	X ₃	(0,a,0)	P4m2	0.0294
(0,1,0)	X ₄	(0,a,0)	P4n2	0.0042
(0,1,0)	X ₅	(0,0,a,b,0,0)	P2 ₁ 2 ₁ 2	0.1140
$(\frac{1}{2}, 1, 0)$	W ₁	(0,0,0,0,-a,a)	I42d	0.0202
$(\frac{1}{2}, 1, 0)$	W ₂	(0,0,0,0,-a,a)	I42d	0.0295

DISCUSSION

It is instructive to compare the phase transitions in other isostructural and isoelectronic lacunar spinels. The particular sequence of phase transitions with decreasing temperature, and low-temperature crystal structures of GaM₄X₈ (M=V, Nb, Ta; X=S, Se) are set by an interplay between JT effects, that act to quench orbital momentum, and spin-orbit coupling on the molecular orbitals, that acts to maintain an orbital character. When the JT effect dominates (M=V) the orbital and magnetic sectors are distinct i.e. a high temperature JT structural transition quenches the orbital degrees of freedom and is preceded by spin ordering at a lower temperature [12, 14, 34, 35]. In both GaV₄S₈ and GaV₄Se₈, the JT distortion selects a ferro polar order with a charge dipole directed along cubic $\langle 111 \rangle$ directions [14, 35]. In the opposite limit of dominant spin-orbit coupling, as is relevant for GaTa₄Se₈, the spin and orbital energy scales

are not separate and the relevant degrees of freedom are spin-orbital entangled $j_{\text{eff}} = 3/2$ states [21, 23]. In this case, there is a single magneto-structural transition at $T^* = 50$ K that cannot be described by a JT active mode [22]. Below T^* , GaTa_4Se_8 enters a valence bond-solid like ground state, and the transition at T^* is driven by interactions between Ta_4 clusters [22] that sets up a staggered arrangement of cluster distortions.

GaNb_4S_8 and GaNb_4Se_8 sit at an intermediate spin-orbit coupling strength, where the interplay between SOC and the JTE becomes most apparent. Since electrons occupy molecular orbitals on cubane (M_4X_4 ; $\text{M}=\text{V}, \text{Nb}, \text{Ta}, \text{X}=\text{S}, \text{Se}$) units in the lacunar spinels, the effective *molecular* spin-orbit coupling is the relevant energy scale. Molecular orbitals are formed from a linear combination of atomic d-orbitals, so the effective spin-orbit coupling strength will increase with increasing transition metal atomic number, but decrease as the M-X orbital hybridization and effective size of molecular orbitals is increased. Thus, the effective spin-orbit coupling strength should be larger in GaNb_4S_8 compared with GaNb_4Se_8 because the broader spatial extent of Se orbitals will enhance M-X hybridization across cubane units. This expectation is borne out through the appearance of only a single transition involving the magnetic and structural degrees of freedom in GaNb_4S_8 , but a separation of energy scales and two transitions in GaNb_4Se_8 . However, unlike the Vanadium compounds, both transitions in GaNb_4Se_8 , at T_Q and T_M , involve rearrangements of Nb_4 clusters and an associated change in the molecular orbital configuration. In other words, the JT transition at T_Q does not act to quench orbital degrees of freedom but instead reduces degeneracy by imposing a staggered quadrupolar order involving spin-orbital moments. As previously pointed out [20], such a transition is similar to the expected quadrupolar ordering predicted for $j = 3/2$ double perovskites [6]; however, we find that quadrupolar ordering in GaNb_4Se_8 is driven by a JT mechanism (ionic motion), rather than intersite orbital exchange.

The JT transition involving spin-orbital degrees of freedom favors an anti polar order in GaNb_4Se_8 [25], with the staggered polar vector oriented along $\langle 111 \rangle$ directions rather than $\langle 111 \rangle$ ferro polar order as in GaV_4S_8 and GaV_4Se_8 [35]. At lower temperatures, a non-JT mechanism results in a rearrangement of the Nb_4 clusters to orient staggered polar order along $\langle 110 \rangle$ directions and form structural dimers. This second transition is similar to the spin-orbital ordering transition at T^* in GaTa_4Se_8 in that it involves distortions that strongly modulate intercluster bonds, and results in an intercluster structural dimerization along $\langle 110 \rangle$ directions. Although the particular staggered pattern of dimers is different between these two compounds, it is likely that both the transition at T^* in GaTa_4Se_8 and at T_M in GaNb_4Se_8 are driven by intercluster spin-orbital interactions.

SUMMARY AND CONCLUSIONS

We have solved crystal structures of GaNb_4Se_8 in the intermediate $T_M < T < T_Q$ and low $T < T_M$ temperature regimes and find that the transitions at T_Q and T_M involve distinct mechanisms. At T_Q , we find a continuous second-order Jahn-Teller, quadrupolar ordering, phase transition on Nb_4 tetrahedron. At $T < T_M$, the unit cell doubles along one axis and forms a singlet dimer state, resembling the sibling compound GaTa_4Se_8 [22]. Compared to previous studies on heat capacity, magnetic susceptibility, and dielectric measurements [20, 25], our results complete the thus far missing structural information for GaNb_4Se_8 . By identifying the structural mechanisms of staggered quadrupolar orderings, these results provide insights into material parameters controlling polar ordering in the orbitally degenerate lacunar spinels. In the future it would be interesting to directly interrogate the spin-and-orbital dynamics in these materials and explore how these energy scales relate to the high pressure superconducting phases in GaTa_4Se_8 and GaNb_4S_8 [4, 26, 36, 37].

Work at Brown University was supported by the U.S. Department of Energy, Office of Science, Office of Basic Energy Sciences, under Award Number DE-SC0021223. This work is based on experiment performed at NSF's ChemMatCARS Sector 15 that is supported by the Divisions of Chemistry (CHE) and Materials Research (DMR), National Science Foundation, under grant number NSF/CHE- 1834750. Use of the Advanced Photon Source, an Office of Science User Facility operated for the U.S. Department of Energy (DOE) Office of Science by Argonne National Laboratory, was supported by the U.S. DOE under Contract No. DE-AC02-06CH11357.

* Current Affiliation: Neutron Scattering Division, Oak Ridge National Laboratory, Oak Ridge, TN 37831, USA

† Corresponding author: kemp_plumb@brown.edu

- [1] William Witczak-Krempa, Gang Chen, Yong Baek Kim, and Leon Balents, "Correlated quantum phenomena in the strong spin-orbit regime," *Annual Review of Condensed Matter Physics* **5**, 57–82 (2014).
- [2] K. W. Plumb, J. P. Clancy, L. J. Sandilands, V. Vijay Shankar, Y. F. Hu, K. S. Burch, Hae-Young Kee, and Young-June Kim, " α - RuCl_3 : A spin-orbit assisted Mott insulator on a honeycomb lattice," *Phys. Rev. B* **90**, 041112 (2014).
- [3] Judit Romhányi, Leon Balents, and George Jackeli, "Spin-orbit dimers and noncollinear phases in d^1 cubic double perovskites," *Physical Review Letters* **118**, 217202 (2017).
- [4] Moon Jip Park, GiBaik Sim, Min Yong Jeong, Archana Mishra, Myung Joon Han, and SungBin Lee, "Pressure-induced topological superconductivity in the spin-orbit Mott insulator GaTa_4Se_8 ," *npj Quantum Materials* **5**,

TABLE III. Crystallographic refinement results at 20, 40 and 100 K.

Temperature (K)	20	40	100
Crystal system	orthorhombic	cubic	cubic
Space group	P2 ₁ 2 ₁ 2 ₁	P2 ₁ 3	F $\bar{4}$ 3m
a (Å)	10.4090(5)	10.4071(6)	10.40910(10)
b (Å)	10.4086(5)	-	-
c (Å)	20.8145(10)	-	-
Data collection diffractometer	15-ID-D, APS	15-ID-D, APS	15-ID-D, APS
Absorption correction	Multiscan	Multiscan	Multiscan
Reflections collected	66929	17258	13368
Independent reflections	16630 ($R_{int}=0.0422$)	2489 ($R_{int}=0.0273$)	464 ($R_{int}=0.0340$)
F(000)	3736.0	1401.0	1868.0
λ (Å, synchrotron)	0.41328	0.41328	0.41328
2 θ range for data collection (deg)	2.544 to 50.64	3.218 to 49.048	3.94 to 47.77
Index ranges	-18 $\leq h \leq$ 19 -19 $\leq k \leq$ 19 -38 $\leq l \leq$ 38	-18 $\leq h \leq$ 18 -13 $\leq k \leq$ 16 -15 $\leq l \leq$ 18	-17 $\leq h \leq$ 15 -19 $\leq k \leq$ 17 -17 $\leq l \leq$ 19
Data, restraints, parameters	16630/0/205	2489/0/41	464/0/12
Goodness of fit	1.088	1.272	1.190
R ₁ , wR ₂ ($I \geq 2\sigma$)	0.0855, 0.1777	0.0442, 0.0776	0.0088, 0.0200
R ₁ , wR ₂ (all)	0.0910, 0.1794	0.0470, 0.0789	0.0088, 0.0200
Largest diff. peak/hole	8.10/-7.15	4.92/-2.54	0.98/-0.96

41 (2020).

- [5] Nan Tang, Yulia Gritsenko, Kenta Kimura, Subhro Bhattacharjee, Akito Sakai, Mingxuan Fu, Hikaru Takeda, Huiyuan Man, Kento Sugawara, Yosuke Matsumoto, Yasuyuki Shimura, Jiajia Wen, Collin Broholm, Hiroshi Sawa, Masashi Takigawa, Toshiro Sakakibara, Sergei Zherlitsyn, Joachim Wosnitzer, Roderich Moessner, and Satoru Nakatsuji, “Spin-orbital liquid state and liquid-gas metamagnetic transition on a pyrochlore lattice,” *Nature Physics* **19**, 92–98 (2023).
- [6] Gang Chen, Rodrigo Pereira, and Leon Balents, “Exotic phases induced by strong spin-orbit coupling in ordered double perovskites,” *Physical Review B* **82**, 174440 (2010).
- [7] W. M. H. Natori, E. C. Andrade, E. Miranda, and R. G. Pereira, “Chiral spin-orbital liquids with nodal lines,” *Physical Review Letters* **117**, 017204 (2016).
- [8] Naoya Iwahara, Veacheslav Vieru, and Liviu F. Chibotaru, “Spin-orbital-lattice entangled states in cubic d¹ double perovskites,” *Physical Review B* **98**, 075138 (2018).
- [9] W. M. H. Natori, M. Daghofer, and R. G. Pereira, “Dynamics of a $j=3/2$ quantum spin liquid,” *Physical Review B* **96**, 125109 (2017).
- [10] Heung-Sik Kim, Jino Im, Myung Joon Han, and Hosub Jin, “Spin-orbital entangled molecular j_{eff} states in lacunar spinel compounds,” *Nature communications* **5**, 3988 (2014).
- [11] Heung-Sik Kim, Kristjan Haule, and David Vanderbilt, “Molecular Mott state in the deficient spinel GaV₄S₈,” *Physical Review B* **102**, 081105 (2020).
- [12] Regina Pocha, Dirk Johrendt, and Rainer Pöttgen, “Electronic and structural instabilities in GaV₄S₈ and GaMo₄S₈,” *Chemistry of Materials* **12**, 2882–2887 (2000).
- [13] Zhe Wang, E. Ruff, M. Schmidt, V. Tsurkan, I. Kézsmárki, P. Lunkenheimer, and A. Loidl, “Polar dynamics at the jahn-teller transition in ferroelectric GaV₄S₈,” *Physical Review Letters* **115**, 207601 (2015).
- [14] E. Ruff, A. Butykai, K. Geirhos, S. Widmann, V. Tsurkan, E. Stefanet, I. Kézsmárki, A. Loidl, and P. Lunkenheimer, “Polar and magnetic order in GaV₄Se₈,” *Physical Review B* **96**, 165119 (2017).
- [15] Ádám Butykai, Sándor Bordács, István Kézsmárki, Vladimir Tsurkan, Alois Loidl, Jonathan Döring, Erik Neuber, Peter Milde, Susanne C. Kehr, and Lukas M. Eng, “Characteristics of ferroelectric-ferroelastic domains in Néel-type skyrmion host GaV₄S₈,” *Scientific Reports* **7**, 44663 (2017).
- [16] Korbinian Geirhos, Boris Gross, Bertalan G. Szigeti, Andrea Mehlin, Simon Philipp, Jonathan S. White, Robert Cubitt, Sebastian Widmann, Somnath Ghara, Peter Lunkenheimer, Vladimir Tsurkan, Erik Neuber, Dmytro Ivaneyko, Peter Milde, Lukas M. Eng, Andrey O. Leonov, Sándor Bordács, Martino Poggio, and István Kézsmárki, “Macroscopic manifestation of domain-wall magnetism and magnetoelectric effect in a Néel-type skyrmion host,” *npj Quantum Materials* **5**, 1–8 (2020).
- [17] K. Geirhos, J. Langmann, L. Prodan, A. A. Tsirlin, A. Missiul, G. Eickerling, A. Jesche, V. Tsurkan, P. Lunkenheimer, W. Scherer, and I. Kézsmárki, “Cooperative Cluster Jahn-Teller Effect as a Possible Route to Antiferroelectricity,” *Physical Review Letters* **126**, 187601 (2021).
- [18] S. Ghara, K. Geirhos, L. Kuerten, P. Lunkenheimer, V. Tsurkan, M. Fiebig, and I. Kézsmárki, “Giant conductivity of mobile non-oxide domain walls,” *Nature Communications* **12**, 3975 (2021).
- [19] O. Arnold, J.C. Bilheux, J.M. Borreguero, A. Buts, S.I. Campbell, L. Chapon, M. Doucet, N. Draper, R. Ferraz Leal, M.A. Gigg, V.E. Lynch, A. Markvardsen, D.J. Mikkelson, R.L. Mikkelson, R. Miller, K. Palmen, P. Parker, G. Passos, T.G. Perring, P.F. Peterson, S. Ren, M.A. Reuter, A.T. Savici, J.W. Taylor, R.J. Taylor,

- R. Tolchenov, W. Zhou, and J. Zikovsky, “Mantid Data analysis and visualization package for neutron scattering and μ SR experiments,” *Nucl. Instr. Meth. Phys. Res. Section A: Accelerators, Spectrometers, Detectors and Associated Equipment* **764**, 156–166 (2014).
- [20] Hajime Ishikawa, Takeshi Yajima, Akira Matsuo, Yoshihiko Ihara, and Koichi Kindo, “Nonmagnetic ground states and a possible quadrupolar phase in 4d and 5d lacunar spinel selenides GaM_4Se_8 ($M=\text{Nb, Ta}$),” *Physical Review Letters* **124**, 227202 (2020).
- [21] Min Yong Jeong, Seo Hyoung Chang, Beom Hyun Kim, Jae-Hoon Sim, Ayman Said, Diego Casa, Thomas Gog, Etienne Janod, Laurent Cario, Seiji Yunoki, Myung Joon Han, and Jung-ho Kim, “Direct experimental observation of the molecular J eff = 3/2 ground state in the lacunar spinel GaTa_4Se_8 ,” *Nature Communications* **8**, 782 (2017).
- [22] Tsung-Han Yang, S. Kawamoto, Tomoya Higo, SuYin Grass Wang, M. B. Stone, Joerg Neufeind, Jacob P. C. Ruff, A. M. Milinda Abeykoon, Yu-Sheng Chen, S. Nakatsujii, and K. W. Plumb, “Bond ordering and molecular spin-orbital fluctuations in the cluster Mott insulator GaTa_4Se_8 ,” **4**, 033123 (2022).
- [23] Thorben Petersen, Pritam Bhattacharyya, Ulrich K Rößler, and Liviu Hozoi, “Resonating holes vs molecular spin-orbit coupled states in group-5 lacunar spinels,” *Nature Communications* **14**, 5218 (2023).
- [24] Stefanie Jakob, Helen Müller, Dirk Johrendt, Sandra Altmannshofer, Wolfgang Scherer, Sudhindra Rayaprol, and Rainer Pöttgen, “Structural and magnetic transitions in the Mott insulator GaNb_4S_8 ,” *Journal of Materials Chemistry* **17**, 3833–3838 (2007).
- [25] M. Winkler, L. Prodan, V. Tsurkan, P. Lunkenheimer, and I. Kézsmárki, “Antipolar transitions in GaNb_4Se_8 and GaTa_4Se_8 ,” *Physical Review B* **106**, 115146 (2022).
- [26] Regina Pocha, Dirk Johrendt, Bingfang Ni, and Mohsen M. Abd-Elmeguid, “Crystal structures, electronic properties, and pressure-induced superconductivity of the tetrahedral cluster compounds GaNb_4S_8 , GaNb_4Se_8 , and GaTa_4Se_8 ,” *Journal of The American Chemical Society* **127**, 8732–8740 (2005).
- [27] G. M. Sheldrick, “A short history of SHELX,” *Acta Crystallographica Section A: Foundations of Crystallography* **64**, 112–122 (2008).
- [28] O. V. Dolomanov, L. J. Bourhis, R. J. Gildea, J. a. K. Howard, and H. Puschmann, “OLEX2: A complete structure solution, refinement and analysis program,” *Journal of Applied Crystallography* **42**, 339–341 (2009).
- [29] “See supplementary material for detail information.”
- [30] Cesar Capillas, Eli Kroumova, Mois I Aroyo, J Manuel Perez-Mato, Harold T Stokes, and Dorian M Hatch, “SYMMODES: A software package for group-theoretical analysis of structural phase transitions,” *Journal of Applied Crystallography* **36**, 953–954 (2003).
- [31] D. Orobengoa, C. Capillas, M. I. Aroyo, and J. M. Perez-Mato, “AMPLIMODES: Symmetry-mode analysis on the Bilbao Crystallographic Server,” *Journal of Applied Crystallography* **42**, 820–833 (2009).
- [32] J. M. Perez-Mato, D. Orobengoa, and M. I. Aroyo, “Mode crystallography of distorted structures,” *Acta Crystallographica Section A* **66**, 558–590 (2010).
- [33] Dan Porter, “DanPorter/Dans_Diffraction: Dans_Diffraction Version 2.2,” (2023).
- [34] C. S. Yadav, A. K. Nigam, and A. K. Rastogi, “Thermodynamic properties of ferromagnetic Mott-insulator GaV_4S_8 ,” *Physica B: Condensed Matter* **403**, 1474–1475 (2008).
- [35] Eugen Ruff, Sebastian Widmann, Peter Lunkenheimer, Vladimir Tsurkan, Sandor Bordács, Istvan Kézsmárki, and Alois Loidl, “Multiferroicity and skyrmions carrying electric polarization in GaV_4S_8 ,” *Science Advances* **1**, e1500916 (2015).
- [36] M. M. Abd-Elmeguid, B. Ni, D. I. Khomskii, R. Pocha, D. Johrendt, X. Wang, and K. Syassen, “Transition from Mott insulator to superconductor in GaNb_4Se_8 and GaTa_4Se_8 under high pressure,” *Physical Review Letters* **93**, 126403 (2004).
- [37] V. Ta Phuoc, C. Vaju, B. Corraze, R. Sopracase, A. Perucchi, C. Marini, P. Postorino, M. Chligui, S. Lupi, E. Janod, and L. Cario, “Optical conductivity measurements of GaTa_4Se_8 under high pressure: Evidence of a bandwidth-controlled insulator-to-metal mott transition,” *Physical Review Letters* **110**, 037401 (2013).